JOURNAL OF AIRCRAFT
Vol. 40, No. 1, January–February 2003

Aerodynamic and Aeroelastic Characteristics of Wings with Conformal Control Surfaces for Morphing Aircraft

B. Sanders*
U.S. Air Force Research Laboratory, Wright–Patterson Air Force Base, Ohio 45433
F. E. Eastep†
University of Dayton, Dayton, Ohio 45469
and
E. Forster‡
U.S. Air Force Research Laboratory, Wright–Patterson Air Force Base, Ohio 45433

Investigations are conducted on lifting surfaces with conventional and conformal trailing-edge control surfaces. The Sohngen inversion formula is used with the thin-airfoil integral equation to determine the aerodynamic pressure for various control surface chord-to-airfoil chord ratios. Comparisons to a conventional control surface show increases in lift and pitching moment of the airfoil with a conformal control surface. Aerodynamic pressure distributions acting on a wing with control surfaces are determined with the vortex lattice technique. Predicted aerodynamic pressures and roll moments are compared to available wind-tunnel data and provide a more general understanding of the aerodynamic behavior observed there. Roll performance of a rectangular wing is determined for various control surface chord-to-wing chord ratios. It is found that the maximum roll rate is greater for a wing with a conformal control surface, but has a lower reversal dynamic pressure than the wing with a conventional control surface. The aerodynamic and aeroelastic results obtained from this investigation provide some insight for wings designed with conformal control surfaces.

Nomenclature

b = semispan
C_{l_p} = rolling-moment coefficient from a unit roll rate
C_{l_β} = rolling-moment coefficient from a unit aileron deflection
c = wing or airfoil chord
c_h = location of control surface hinge line aft of leading edge
p = roll rate
t = wing thickness
U = velocity
z_c = airfoil mean camber line
α = aerodynamic angle of attack
β = flap deflection angle
ξ = chordwise location where the downwash condition is satisfied in an aerodynamic panel (for example, $\frac{3}{4}$ chord point of each panel)

Subscripts

cf = conformal control surface
cv = conventional control surface

Introduction

AIR vehicles are optimized for specific flight conditions (that is, low drag, roll performance). When the vehicle operates away from this design point, the performance will decline. The ability to adapt air vehicle aerodynamic shape to increase the optimum flight envelope is therefore highly desirable. This is an elusive goal that aircraft designers continually strive to achieve and keep technologists motivated to invent new and innovative adaptive structure concepts.

Aircraft have always been adaptive in one form or another, and aerospace history is rich with innovative solutions to this design issue. For example, the Wright brothers used wing warping, an adaptable lifting surface, to control the Wright B flyer. As aircraft speed increased, wings became stiffer to preclude aeroelastic instabilities (for example, divergence, flutter). Wing warping disappeared because the power required exceeded actuator capabilities, and the more energy efficient aileron system emerged, which is just another form of shape adaptation. Other forms of shape control for aerodynamic performance are retractable landing gear, flaps, and trim tabs. These have all been successfully fielded and are predominant in modern day vehicle design from general aviation aircraft to high-performance military aircraft. More advanced forms of shape control include wing sweep, camber changes, and wing twist.

Wing sweep is used to optimize the vehicle configuration for current flight conditions. Wings are swept to strike a balance between range and speed by delaying the rise in drag as the vehicle speed increases. Most applications of wing sweep are done in a symmetric fashion. Examples include several military aircraft, such as the F-111 Aardvark, B1 Lancer, and the F-14 Tomcat. Robert T. Jones[1] introduced the notion of an oblique wing to enhance high-speed cruise performance of commercial aircraft. In this case the entire wing is rotated around a central point on the fuselage, and so the sweep is antisymmetric. Jones showed that a transport-sized aircraft equipped with an oblique wing would have substantially better aerodynamic performance than aircraft with conventional wings up to a Mach number of 1.4.

Another highly sought after shape control concept is variable camber. In addition to ailerons to control roll performance, this is currently accomplished using articulated, trailing-edge flaps to increase the lift coefficient during slow speed flight. Several innovative techniques have been introduced to achieve this.[2] In the 1970s the Mission Adaptive Wing[3] program demonstrated an inventive technique to modify the wing camber in flight. It was demonstrated

Received 23 March 2001; presented as Paper 2001-1211 at the AIAA 42nd Structures, Structural Dynamics and Materials Conference, Seattle, WA, 16–19 April 2001; revision received 10 April 2002; accepted for publication 14 May 2002.

*Research Engineer, Air Vehicles Directorate, Structures Division. Associate Fellow AIAA.
†Professor Emeritus, Department of Mechanical and Aerospace Engineering. Fellow AIAA.
‡Research Engineer, Air Vehicles Directorate, Structures Division. Member AIAA.

on the F-111. A design using existing hydraulic actuation and mechanical linkages enabled the wing to have a smoothly varying camber in the chordwise direction. Some spanwise variation was also enabled by this design. A flight-test program was completed, and data were obtained about the system performance in and around the transonic flight regime.

One of the more innovative concepts for shape control that has emerged over the last two decades is Active Aeroelastic Wing (AAW) Technology.[4] AAW is a design concept that utilizes multiple leading-edge and trailing-edge control surfaces to advantageously use wing twist to increase several vehicle performance metrics. Wind-tunnel and analytical studies have shown that this technology can significantly improve aerodynamic performance while reducing weight for air vehicles expected to operate in the subsonic and supersonic flight regimes.

A cursory search of patents and the literature reveals an abundance of other pioneering adaptive wing concepts such as telescoping wings to increase wing area and variable thickness to improve cruise performance in the transonic regime. Most of these concepts have never been fielded because of, among other things, unacceptable weight increases associated with the actuation systems and the lack of efficient structures with desirable and controllable deformation characteristics.

Recent advancements in actuation and sensing technology have reinvigorated the exploration of adaptive aerospace structures. In the last 10 years several investigations have been conducted to understand the application of smart materials to control of air vehicle structures. Smart material based actuation systems are attractive because of their characteristic high-energy densities. Ehlers and Weisshaar[5] conducted a comprehensive analytical study to understand how active control using piezoelectric (PZT) patches to reshape the wing can improve aerodynamic performance and control static aeroelastic characteristics such as divergence. Lin et al.[6] conducted a highly innovated experimental and analytical investigation to increase the aircraft flight envelop by suppressing flutter using a distributed network of piezoelectric patches. The practical application of PZT actuators to control flutter for actual air vehicles has not yet been done. However, these studies, and several like them,[7–9] have shown that a network of sensors and actuators could be used to control a structure and improve the flight performance of air vehicles. When applied to a vehicle design, these concepts might enable efficient multipoint operation of air vehicles and potentially efficient multimission vehicles. NASA and the Defense Advanced Research Projects Agency have adopted the term of "morphing aircraft" to describe the application of adaptive structures, among other technologies, for this purpose.

Several advancements in technology and understanding need to be made before these morphing concepts can be applied to air vehicles. This includes, but is not limited to, obtaining an understanding of how to design aircraft structures efficiently to be controlled by a network of actuators, the development of high-energy density actuators with characteristics that match air vehicle needs, efficient integration of these actuation concepts into the structure to achieve minimum energy requirements, and understanding the aerodynamic performance of these adaptive structure concepts.

This paper investigates one aspect of a smart material based technology that may be applicable to the design of a morphing aircraft. It addresses the concept of conformal control surfaces for aerodynamic control. A wind-tunnel demonstration of a wing with embedded smart materials was recently completed.[10] The goal of this program was to demonstrate how smart materials integrated into a scaled typical fighter aircraft wing impacts aerodynamic performance. The model used shape memory alloy (SMA) torque tubes to actively twist the wing and SMA wires to smoothly deform trailing-edge control surfaces (that is, conformal control surface). Measurements of various aerodynamic coefficients, such as the coefficient of lift and pitching moment, were taken. The purpose of this paper is to complement this wind-tunnel program with an analytical investigation and provide a broader understanding of the experimental findings and their potential impact on wing design.

Wind-Tunnel Model

The purpose of this section is to provide highlights of the wind-tunnel model and how they are addressed in the analysis. A schematic of the wind-tunnel model is shown in Fig. 1. It is a 16% scale model of a F-18 aircraft wing. The model has a maximum t/c of 6% at the root and 4% at the wing tip with a wing sweep of 29 deg. This is a supersonic wing with airfoil camber, but it is modeled as a flat plate for this study. Finally, the snare, located at

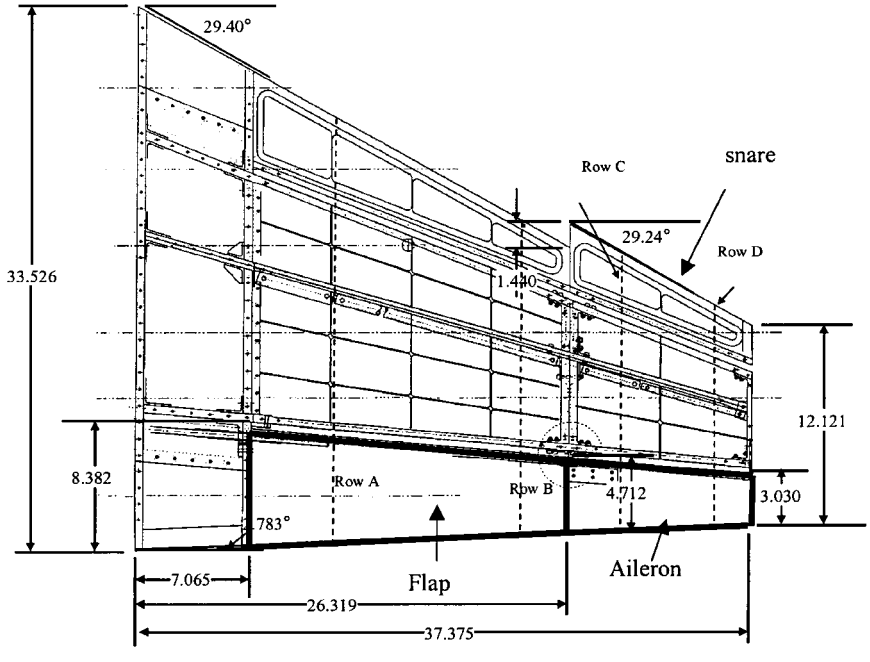

All linear dimensions in inches

Fig. 1 Schematic of smart wing program phase 1 wind-tunnel model.

the outboard section of the leading edge, is not included in the aerodynamic analysis. More detail on the model design, fabrication, and the experimental program can be found in Refs. 11 and 12.

Two models are fabricated for testing, one with conventional control surfaces and one with conformal control surfaces. Each model has two control surfaces: a flap and an aileron. The control surface chord-to-wing chord has a ratio of approximately 25%. On each model the flaps and ailerons have the same dimensions. The dynamic and structural characteristics (for example, GJ and EI) for each model are identical. The models are considered to be sufficiently stiff to warrant a rigid-body assumption.

Aerodynamic Methods

The maximum t/c for each wing is on the order of 6%. Additionally, the available experimental data are for Mach numbers less than 0.3, and, for the most part, the angle of attack α and flap deflection angles β are much less than 0.1 radian. These conditions are consistent with the assumptions for linear, invisid, small disturbance theory.[13] Thus, linear potential aerodynamic tools are considered suitable for this investigation.

The Sohngen inversion formula[14] and the vortex lattice method[15] (VLM) are used to compute pressures on the airfoil and rigid wing, respectively, whereas ASTROS®[16] is used for the aeroelastic analysis. Analytical solutions of the Sohngen inversion are obtained using Mathematica®. A key element in this analysis is the evaluation of the downwash condition on the airfoil surface:

$$w = U_o\left(\alpha - \frac{\mathrm{d}z_c}{\mathrm{d}x}\right) \tag{1}$$

For a flat-plate airfoil, or wing, with a conventional, or articulated, trailing-edge control surface, the slope of the camber line has the form:

$$\frac{\mathrm{d}z_c}{\mathrm{d}x} = \begin{cases} 0 & \text{for} \quad x < c_h \\ \beta & \text{for} \quad x \geq c_h \end{cases} \tag{2}$$

Where β is the control surface deflection, which is positive in the downward direction.

Experimental measurements of the shape of the deflected conformal control surfaces in the wind tunnel are not available. The only available data from the wind tunnel are the deflection angle of the articulated control surface and the secant angle of the conformal control surface, which is measured from the leading edge to the trailing edge of the control surface. However, a finite element model of a control surface fabricated with SMA wires is available to provide information about the deformed shape. Figure 2 shows results obtained from a finite element analysis for a typical section. For this study the shape is approximated as a parabolic arc, which is also shown in Fig. 2.

A similar control surface deflection must be selected to compare the aerodynamic performance of the two control surfaces. The displacement of the trailing edge of the control surface is chosen here. The downwash condition for the conformal control surface is formulated in terms of the secant angle formed between the leading and trailing edge of the control surface. This is the equivalent to the angle β. For a typical section using this type of control surface, it can be shown that the slope of mean camber line is

$$\frac{\mathrm{d}z_c}{\mathrm{d}x} = \begin{cases} 0 & \text{for} \quad x < c_h \\ -2\beta\left(\dfrac{\xi/c - c_h/c}{(1 - c_h/c)}\right) & \text{for} \quad x \geq c_h \end{cases} \tag{3}$$

For small deflections this approach is reasonable.

Airfoil Performance

Figure 3 shows the results of the two-dimensional analysis for an airfoil with either a conventional or a conformal trailing-edge control surface. Two flap-to-chord ratios are selected, 50% and 10%, to illustrate the effect on the pressure distributions. The two-dimensional analysis shows the relationship of the chordwise pressure distribution across the airfoil for the control surface and provides a good understanding of the effects of airfoil geometry. Forward of the hinge line the pressure distribution is higher for the conformal control surface. Another notable difference in the pressure distribution is in the area around and aft of the hinge line. The articulated surface shows the classic pressure spike caused by the abrupt change in the direction of flow. On the other hand, the pressure distribution on the conformal surface reaches a maximum behind the hinge line but does not have a pressure spike associated with it. The elastic axis for a flexible wing is typically around 30–40% aft of the leading edge, and the pressure distribution produced by the conformal control surface will result in a larger leading-edge-down pitching moment about the elastic axis. The performance implications of this characteristic on flexible wings are discussed later.

The effect on the aerodynamic performance resulting from these pressure distributions can be quantified by comparing the aerodynamic coefficients, which are shown in Figs. 4 and 5 as a function of the flap-to-chord ratio. Figure 4 shows the variation in sectional lift coefficient C_l. The increase in lift coefficient for the conformal control surface is approximately 40% over entire range considered. Figure 5 shows the variation in pitching moment C_m about the aerodynamic center (for example, the $\frac{1}{4}$ chord). The maximum

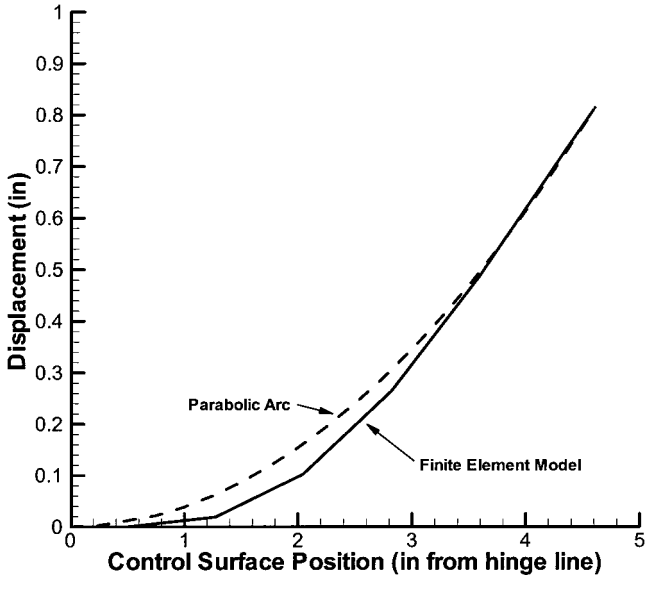

Fig. 2 Typical SMA-based control surface deflection—FEM vs parabolic arc.

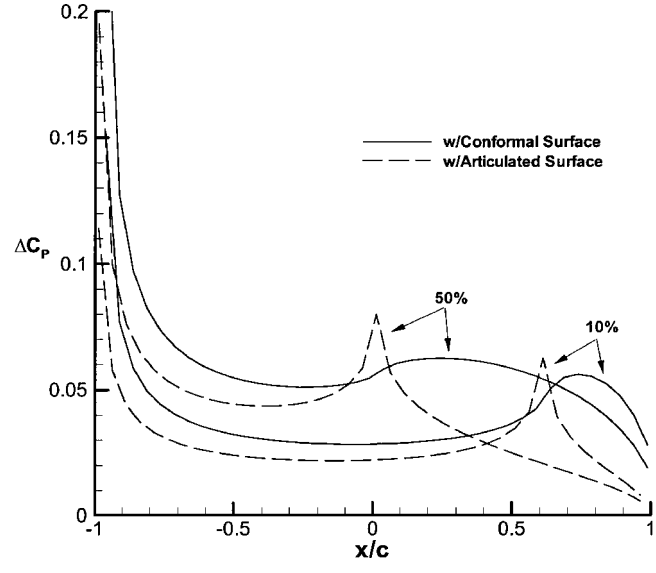

Fig. 3 Pressure distribution over an airfoil as a function of two control surface geometries and two flap-to-chord ratios: 10 and 50%.

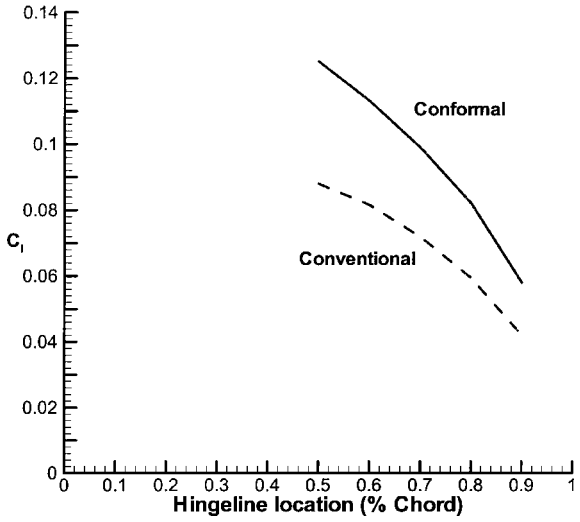

Fig. 4 C_l **vs hinge-line location for an airfoil with a trailing-edge control surface.**

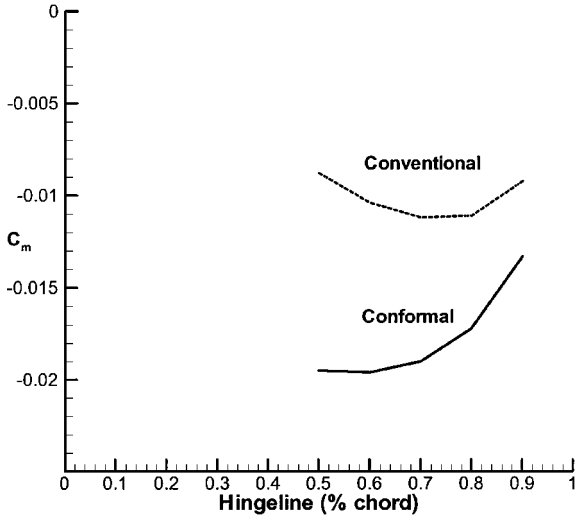

Fig. 5 C_m **vs hinge-line location for an airfoil with a trailing-edge control surface.**

pitching moment for airfoil with the conventional control surface occurs when the hinge line is around 75% of the chord (for example, flap-to-chord ratio of 25%). On the other hand, the conformal control surface produces an increasing negative pitching moment over most of the range considered. A peak value is obtained when the hinge line is around 60% and decreases only slightly after that.

Higher-order shapes of the control surface are also investigated. Figure 6a compares the shapes of different control surfaces using linear, second-order (parabolic), third-order, and fourth-order functions, and Fig. 6b shows the resulting pressure distributions. It shows that higher-order deformations of the control surface further enhance the aerodynamic effects. For example, the pressure distribution is increased, which will lead to higher lift coefficients. The peak pressure also occurs further aft as the order of the camber-line model is increased and a further exasperation of the nose-down pitching moment just discussed occurs. This will result in a higher pitching moment about the aerodynamic center. For the remainder of this investigation, the parabolic arc approximation is used as the model for the conformal control surface.

These results demonstrate that not only can improvements in lift be obtained with a conformal control surface but increases in roll performance are possible too. However, care must be taken when designing a wing with this type of control surface because aileron reversal will occur at lower dynamic pressure as a result of the negative increase in pitching moment. This is discussed in more detail later in the paper.

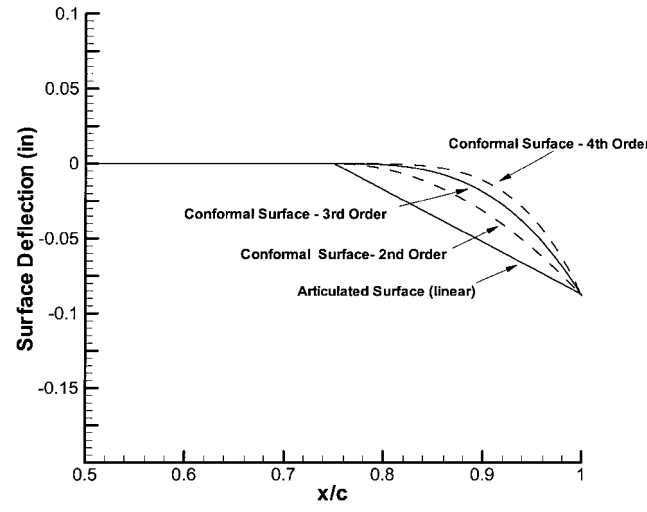

Fig. 6a Control surface shapes for four surface geometries.

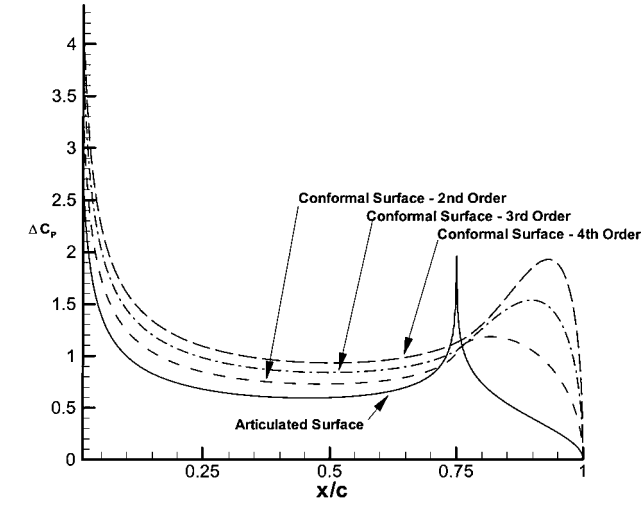

Fig. 6b Pressure distribution over an airfoil as a function of four control surface geometries.

Wing Performance

The VLM provides a deeper understanding of the experimental data generated during the Smart Wing wind-tunnel test. An aerodynamic analysis is conducted on a rigid structural model of the F-18 wing to study the trends in pressure distribution and roll-moment coefficients measured in the wind tunnel.[10] Additionally, an aeroelastic analysis is conducted to understand the impact of the aerodynamic characteristics of the conformal control surfaces on the roll performance.

Rigid-Wing Roll Performance

A comparison of the C_L vs α curve is made of the clean wing (for example, no surface deflections) to establish a baseline for other comparisons. The results are presented without reference to a figure. The experimental data are linear up to an angle of attack of 10 deg, which is the primary region of interest for this study. The slopes of the C_L vs α curves match very well, as shown:

$$\frac{dC_L}{d\alpha} = \begin{cases} 0.060 & \text{VLM} \\ 0.057 & \text{EXP} \end{cases}$$

This result indicates that excluding the snare in the aerodynamic model is a reasonable approximation for the small angles of attack of interest in this study. Although the slopes are similar, at a 0-deg angle of attack there is an offset for the wind-tunnel model. A lift coefficient of -0.02 is measured at this condition. This is most likely a result of some small amount of twist built into the model.

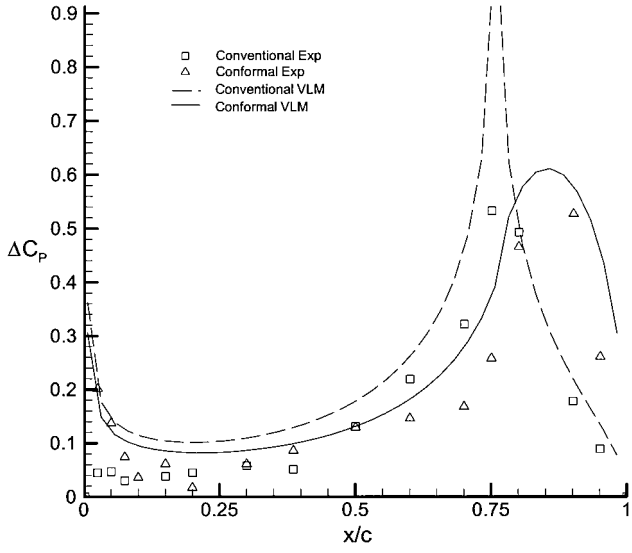

Fig. 7 Pressure distribution over wing at $\alpha = 0$ deg, $\beta_{cv} = 10$ deg, $\beta_{cf} = 7$ deg.

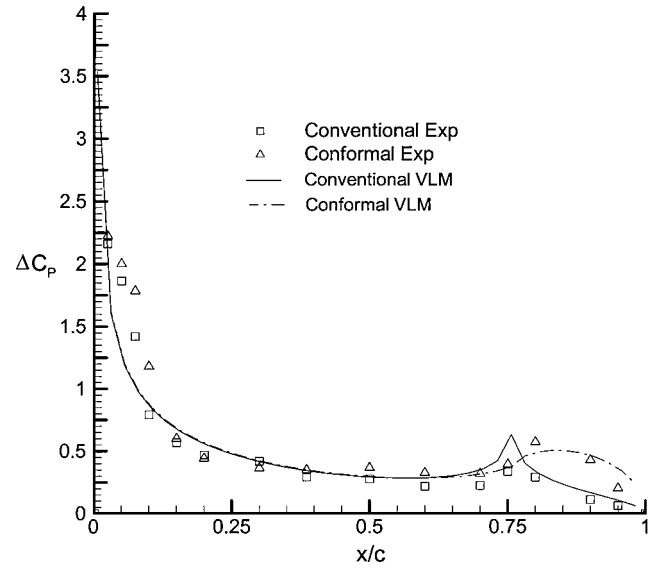

Fig. 8 Pressure distribution over wing at $\alpha = 6$ deg, $\beta_{cv} = 10$ deg, $\beta_{cf} = 7$ deg.

Because of scatter in the data and complications with the experimental equipment, it is difficult to understand trends in the pressure data from the experimental data itself. However, the VLM aids in "filling in the gaps" and more clearly illustrates the trends in the pressure distributions. Figure 7 shows typical variations in the ΔC_p vs x/c obtained from the VLM and experiment. The data are taken from a spanwise station located on the aileron, which is indicated as row D in Fig. 1. Pressure data are not available for equal deflection angles of the ailerons, so that a case is selected where the deflections angles are close. For the case shown in Fig. 7, the aileron is deflected 10 deg when the model is configured with the conventional control surface β_{cv} and deflected 7 deg when the model is configured with the conformal control surface β_{cf}. The angle of attack in each case is 0 deg. The lines show the pressure distributions predicted from the VLM, and the experimental data are represented by the open symbols. Crimping of pressure tubes is the source of erratic measurements at the leading edge. Particular attention should be focused in the area around and aft of the control surface hinge line ($x/c > 0.75$). Similar to the two-dimensional case discussed before, the pressure distribution associated with the conformal control surface shows a peak aft of the conventional surface, whereas the conventional control surface shows signs of the classical pressure spike at the hinge line.

Figure 8 shows a similar comparison at an angle of attack of 6 deg. Again, exact control surface deflections are not available for the two configurations, and the data are taken from a spanwise station located on the aileron, which is indicated as row D in Fig. 1. The variation in the experimental data is more clearly observed in this figure, which is highlighted by the VLM. At this angle of attack the leading-edge pressure peak dominants the pressure distribution across the wing. Even though the conventional flap is deflected 3 deg more, the pressure difference forward of the hinge line is nearly equal at all of the pressure taps. The few that are not are considered a result of experimental scatter. This suggests that for equal deflection angles the distribution would be the same as that shown earlier in the two-dimensional analysis.

Figure 9 shows the results of VLM and the experimental data for the roll-moment coefficient. In this case the aileron (conventional and conformal) is deflected 10 deg. It can be observed that the roll moment is consistently higher for the wing configured with the conformal control surface. This observation is consistent with what the two-dimensional analysis would suggest for a rigid wing. The VLM overpredicts the roll moment. This is consistent with the offset observed in the wind-tunnel model for the clean wing condition as described earlier. Despite this, it is able to verify the increase, or difference, in roll moment obtained with the conformal control surface, which is illustrated by the horizontal line.

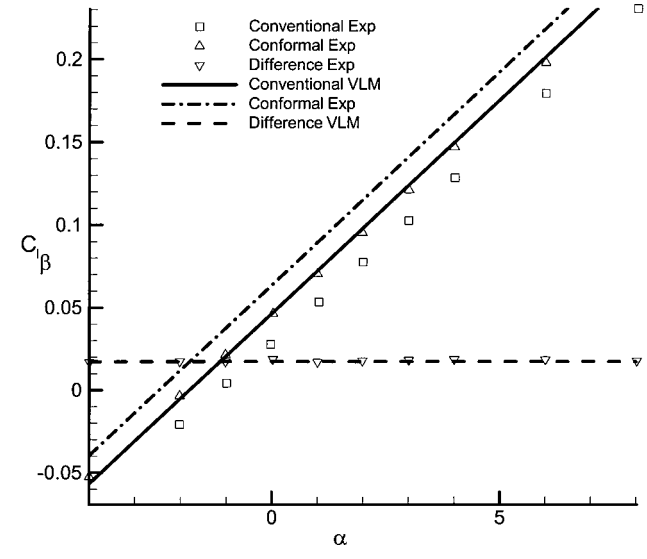

Fig. 9 C_{l_β} vs α; aileron deflected only $\beta_c = 10$ deg, $\beta_s = 10$ deg.

Aeroelastic Roll Response

In addition to understanding the aerodynamic performance, we are interested in understanding the roll characteristics of wings with these control surfaces. As mentioned earlier, the rigid-body two-dimensional aerodynamic analysis shows that the nose-down pitching moment is much larger for the airfoil with the conformal control surface. This will affect the roll performance of flexible wings.

For this component of the analysis, a cantilevered, straight wing is selected.[17] The aerodynamic planform has a 6-ft chord and a 20-ft semispan. A beam representation is selected for the structure and is modeled using 10 finite element segments. It has the following structural properties: $EI = 23.6 \times 10^6$ lb-ft^2, $GJ = 2.39 \times 10^6$ lb-ft^2, $S_y = 0.447$ slug-ft/ft, $I_y = 1.943$ slug-ft^2/ft, $m = 0.746$ slug/ft. The elastic axes and center of mass are located at positions 34 and 43%, respectively, of the chord aft of the leading edge. Three different flap-to-wing chord ratios are selected for analysis: 50, 25, and 10%. The spanwise location of the aileron is from 75% of the span to the wing tip. Figure 10 shows a typical aerodynamic grid overlayed on the finite element structural model of the wing. Bold lines show the location of the aileron. ASTROS is used to solve for the static aeroelastic response at a sea-level condition with a Mach number of

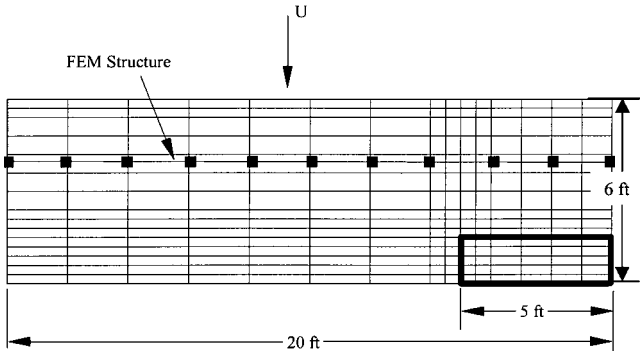

Fig. 10 Typical structure and aerodynamic model for aeroelastic analysis.

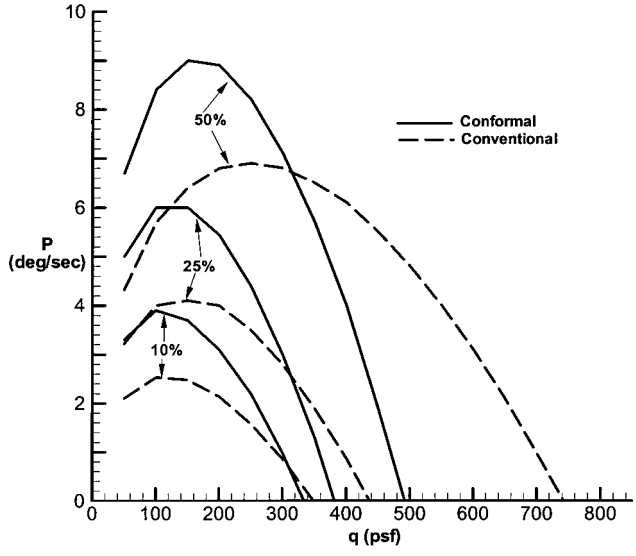

Fig. 11 Roll performance of a flexible wing as a function of three flap-to-wing-chord ratios: 10, 25, and 50%.

zero. In this case we are only interested in the roll rate as a function of the dynamic pressure.

Figure 11 shows a plot of the roll rate p about the longitudinal x axis in degrees/second for the flexible straight wing. The roll rate is determined for a 1-deg aileron deflection using

$$p = -\left(C_{l_\beta} / C_{l_p}\right)(2U/b)\beta \tag{4}$$

We already mentioned that the conformal control surface produces an increase in the lift coefficient and a more negative pitching moment. This effect on the wing roll performance is illustrated here. It is observed that the maximum roll rate is increased on the order of 25–30% when using a conformal control surface. This is a result of the total increase in lift produced on the wing section when using these control surfaces, as shown in Fig. 3. Also, the peak roll rate occurs at lower dynamic pressures with the conformal surface. The dynamic pressure for roll reversal is higher for the wing configured with the conventional control surface, which is an artifact of the larger negative pitching moment that develops with the conformal surfaces. This behavior has been observed in recent experiments,[18] and the general aeroelastic effect was observed in the AFTI/F-111 wind-tunnel demonstration.[19] The difference in reversal pressure becomes smaller as the flap-to-wing chord ratio is reduced. These features need to be taken into account when considering conformal control surfaces for wing design.

Summary

This paper investigated aerodynamic and aeroelastic performance metrics that affect roll performance for wings with articulated and conformal control surfaces. These smoothly varying surfaces may be appropriate for design through the use of advanced activation and mechanization concepts. Rigid and elastic structures and linear aerodynamic theories are used to analyze the improvements in aerodynamic coefficients. The results of the analysis are compared to experimental results obtained from a 16% scale model of a typical fighter wing with embedded smart materials to deform a control surface. This study supports the experimental findings that a conformal control surface has some distinct aerodynamic benefits as compared to a conventional control surface and provides clearer definition about the trends in the pressure distribution over the wing. Also, some insight into the behavior of flexible wings designed with these control surfaces is described. The current design of the control surfaces could work well for low rate applications (for example, takeoff and landing configurations). This concept will be ideal for multiple control surface concepts, such as active aeroelastic wing technology, when actuators with increased bandwidth are developed.

References

[1]Jones, R. T., "The Minimum Drag of Thin Wings in Frictionless Flow," *Journal of Aeronautical Science*, Vol. 18, No. 2, 1951, pp. 75–81.

[2]Abbott, I. H., and Von Doenhoff, A. E., *Theory of Wing Sections*, Dover, New York, 1959, pp. 188–246.

[3]Hall, J. M., "Executive Summary AFTI/F-111 Mission Adaptive Wing," WRDC-TR-89-2083, Sept. 1989.

[4]Pendleton, E., Bessette, P., Field, P., Miller, G., and Griffin, K., "Active Aeroelastic Wing Flight Research Program: Technical Program and Model Analytical Development," *Journal of Aircraft*, Vol. 37, No. 4, 2000, pp. 554–561.

[5]Ehlers, S. M., and Weisshaar, T. A., "Static Aeroelastic Control of an Adaptive Lifting Surface," *Journal of Aircraft*, Vol. 30, No. 4, 1993, pp. 534–540.

[6]Lin, C. Y., Crawley, E. F., and Heeg, J., "Open- and Closed-Loop Results of a Strain-Actuated Active Aeroelastic Wing," *Journal of Aircraft*, Vol. 33, No. 5, 1996, pp. 987–994.

[7]Liu, Y., Kapania, R. K., Gern, F. H., and Inman, D. J., "Equivalent Plate Modeling of Arbitrary Wings," *Proceedings of the International Conference on Computational Engineering and Sciences*, Vol. 2, 2000, pp. 515–521.

[8]Khot, N. S., Eastep, F. E., and Kolonay, R. M., "Method for Enhancement of the Rolling Maneuver of a Flexible Wing," *Journal of Aircraft*, Vol. 34, No. 5, 1997, pp. 673–678.

[9]Henderson, D., Moses, R. W., Ryall, T., and Zimcik, D., "Overview of an Active Buffeting Alleviation System," *CEAS/AIAA/ICASE/NASA Langley International Forum on Aeroelasticity and Structural Dynamics*, 1999, pp. 615–625.

[10]Kudva, J. N., "Overview of the DARPA/AFRL/NASA Smart Wing Program," *Society of Photo-Optical Instrumentation Engineers Conference on Industrial and Commercial Applications of Smart Structures Technologies*, Vol. 3674, 1998, pp. 21–30.

[11]Martin, C. A., "Design and Fabrication of Smart Wing Tunnel Model and SMA Control Surfaces," *Society of Photo-Optical Instrumentation Engineers Conference on Industrial and Commercial Applications of Smart Structures Technologies*, Vol. 3674, 1988, pp. 31–40.

[12]Scherer, L. B., "DARPA/AFRL/NASA Smart Wing Second Wind Tunnel Tests Results," *Society of Photo-Optical Instrumentation Engineers Conference on Industrial and Commercial Applications of Smart Structures Technologies*, Vol. 3674, 1998, pp. 41–49.

[13]Anderson, J. D., *Fundamentals of Aerodynamics*, McGraw–Hill, New York, 1984, pp. 189–274.

[14]Bisplinghoff, R. L., Ashley, H., and Halfman, R. L., *Aeroelasticity*, Addison Wesley Longman, Reading, MA, 1955, pp. 217, 218.

[15]Bertin, J. J., and Smith, M. L., *Aerodynamics for Engineers*, Prentice–Hall, Upper Saddle River, NJ, 1998, pp. 291–311.

[16]Johnson, E. H., and Neill, D. J., "Automated Structural Optimization System (ASTROS), Volumte III-Applications Manual," U.S. Air Force Research Lab., TR-88-3028, Wright–Patterson AFB, OH, Dec. 1998.

[17]Goland, M., "The Flutter of a Uniform Cantilevered Wing," *Journal of Applied Mechanics*, Dec. 1945, pp. A197–A208.

[18]Sanders, B., Martin, C. A., and Cowan, D., "Aerodynamic and Aeroelastic Characteristics of the DARPA Smart Wing Phase II Wind Tunnel Model," *Society of Photo-Optical Instrumentation Engineers Conference on Industrial and Commercial Applications of Smart Structures Technologies*, Vol. 3674, 2001, pp. 301–311.

[19]Nelson, D. W., "AFTI F-111 Aerodynamics," U.S. Air Force Research Lab., AFRL-TR-78-3026, July 1987.